Spinodal Stratification in Ultrathin Micellar Foam Films

Journal:	*Molecular Systems Design & Engineering*
Manuscript ID	ME-ART-12-2018-000102.R1
Article Type:	Paper
Date Submitted by the Author:	23-Feb-2019

Complete List of Authors:	Yilixiati, Subinuer; University of Illinois at Chicago, Department of Chemical Engineering Wojcik, Ewelina; University of Illinois at Chicago, Department of Chemical Engineering Zhang, Yiran; University of Illinois at Chicago, Department of Chemical Engineering Sharma, Vivek; University of Illinois at Chicago, Department of Chemical Engineering

Spinodal Stratification in Ultrathin Micellar Foam Films

Subinuer Yilixiati, Ewelina Wojcik, Yiran Zhang and Vivek Sharma*

Department of Chemical Engineering, University of Illinois at Chicago, IL.

*Corresponding author: viveks@uic.edu

Submitted on November 29th, 2018, Revised on Feb 23rd, 2019

ABSTRACT

We report the discovery of a hitherto unreported mechanism of drainage and rupture of micellar foam films that presents unexplored opportunities for understanding and controlling the stability, lifetime and properties of ubiquitous foams. It is well-known that ultrathin micellar foam films exhibit stratification, manifested as stepwise thinning and coexistence of thin-thick flat regions that differ in thickness by a nanoscopic step size equal to the intermicellar distance. Stratification typically involves the spontaneous formation and growth of thinner, darker, circular domains or thicker, brighter mesas. Mechanistically, domain expansion appears similar to hole growth in polymer films undergoing dewetting by nucleation and growth mechanism that can be described by considering metastable states resulting from a thickness-dependent oscillatory free energy. Dewetting polymer films occasionally phase separate into thick and thin regions forming an interconnected, network-like morphology by undergoing spinodal dewetting. However, such thick-thin patterns, that we term spinodal stratification, have never been reported for freestanding films. In this contribution, we show that spinodal stratification can occur in both single foam films and in bulk foam. We visualize and characterize the nanoscopic thickness variations and transitions by using IDIOM (Interferometry Digital Imaging Optical Microscopy) protocols to obtain AFM-like exquisite thickness maps of freestanding films. We show that the origin of spinodal stratification is the thickness-dependent oscillatory contribution to free energy that arises due to confinement-induced layering of micelles, and we find that evaporation and enhanced drainage in vertical films play a critical part in driving the process.

Design, System, Application

We pursue an understanding of molecular principles that are critical for understanding and controlling the stability and lifetime of foams. Foam films typically consist of fluid sandwiched between two surfactant-laden surfaces that are ~ 5 nm - 10 microns apart, and the drainage in films occurs under the influence of viscous, interfacial and intermolecular forces, including disjoining pressure. Drainage in foam film formed by surfactant concentrations above the critical micelle concentration proceeds in a non-monotonic, step-wise fashion called stratification. Using unprecedented experimental insights obtained from the interferometry, digital imaging and optical microscopy (IDIOM) protocols we developed recently, we elucidate the role of supramolecular oscillatory structural force contribution in causing stratification that typically occurs by nucleation and growth of thinner darker domains. Such thinner domains are thinner than surrounding flat film by a step-size proportional to intermicellar distance, and the coexisting thick-thin regions are considered to be multiple metastable states that arise as a consequence of thickness-dependent free energy functional. Thermodynamically, such an oscillatory free energy functional ought to make the freestanding films susceptible to spinodal-like phase separation into thick and thin regions, though such patterns have never been reported before. In this study, we report the discovery and analysis of spinodal stratification, outline the role of micellar interactions and disjoining pressure, and highlight the opportunities and challenges for molecular engineering of foams.

INTRODUCTION

In 1966, Vrij[1] examined the theoretical expression for the free energy of ultrathin films (thickness <100 nm) and argued that ultrathin films can form spinodal-like patterns with distinct thick and thin regions due to non-monotonic dependence of free energy on film thickness. Vrij[1] suggested an analogy with liquid mixtures undergoing compositional phase separation by spinodal decomposition (first described by Cahn[2] in 1965). It is well-established that supported ultrathin films can undergo dewetting[3-7] can form thick-thin network-like patterns anticipated by Vrij.[1] Indeed, controlling, analyzing and understanding dewetting pattern formation are problems of continued technical interest for creating nanoscopic films (or structures) for application in microelectronics, medicine and photovoltaics[7-16] and of fundamental curiosity and interest due to the role played by confinement, nanofluidics and intermolecular and surface forces.[1-26] However, the formation of such spinodal thick-thin regions in foam films or freestanding films have not been reported in the literature for the last fifty-one years, and the mechanism for rupture of foam films proposed by Vrij[1] remains uncorroborated. Using experiments and theory, Derjaguin and coworkers[27-30] in the 1940s and 1950s first recognized that the free energy change associated with differential change in thickness gives rise to a measurable disjoining pressure that influences flows, stability and lifetime of freestanding and supported ultrathin films. Vrij[1] considered the free energy expression for thin films by accounting for disjoining pressure contributed by van der Waals and electrostatic double layer surface forces (known together as DLVO forces[27, 31, 32]). However, Vrij[1] never considered the possibility of spinodal-like patterns arising in the presence of the non-DLVO, supramolecular oscillatory structural contribution to disjoining pressure that

arises in foam films containing supramolecular structures like micelles, nanoparticles, liquid crystalline phases, lipid bilayers or polyelectrolytes.[33-40] In this study, we report the discovery, visualization and analysis of spinodal stratification, associated with the spontaneous appearance of thick-thin regions, or nanoscopic 'hills and gullies' in freely draining, micellar foam films. Due to analogies with both spinodal dewetting and spinodal phase separation, we have christened the process as spinodal stratification.

The fragile beauty of bubbles, foams, and soap films fascinates scientists, poets, painters, children, and the curious alike.[41-46] For example, Carl Sandberg's three line poem titled *Bubbles* says: Two bubbles found they had rainbows in their curves./ They flickered out saying:/ "It was worth being a bubble just to have held that rainbow thirty seconds." A freshly created soap bubble (or a soap film) displays iridescent colors under white light illumination due to thin film interference; however, the interference colors disappear below 100 nm, and progressively thinner films manifest with progressive darker shades of gray.[30, 41-45] The underlying problem of stability, flow (drainage) and rupture in thin liquid films is of immense practical importance for understanding properties of foams and emulsions,[41-48] and for quantifying the magnitude and influence of intermolecular and surface forces.[27, 30, 31, 34-36, 49-54] In ultrathin foam films, intermolecular and surface forces contribute a thickness-dependent disjoining pressure that can counterbalance the suction flows created by Laplace pressure, and stabilize films against rupture, extending foam stability.[27, 30, 31, 34-36, 42-54] Scientists like Hooke,[55] Newton,[56] and Brewster[57] (also see the classical soap film references[41-46]) had observed that drainage of soap films leads eventually to appearance of black films. Even though the existence of two blacks was well-known by the end of the nineteenth century, it was

not known that soap films contain surfactants that spontaneously adsorb to liquid-air interface reducing surface tension and altering interfacial rheology response, and also self-assemble within bulk fluid to form supramolecular structures called micelles above a critical micelle concentration (CMC).[58] It is now well-understood that the two blacks (common black and Newton black) thicknesses can arise in foam films formed with ionic surfactants, with concentrations below CMC, [31, 42, 43, 59] and the thicknesses can be computed using DLVO theory.

Johonnott[60] in 1906 first reported the existence of multiple blacks, and determined that the coexistence of regions with distinct shades of grey implies that soap films are stratified. Johonnott used interferometry to determine the drainage involved step-wise thinning with time, and a decade later, Perrin[61, 62] too observed stratification in experiments with soap films, and cited stratification as an evidence for molecular reality in his Nobel lecture. Decades later, Bruil and Lyklema[63] rediscovered stratification in 1971, and reported that concentration-dependent step size for sodium dodecyl sulfate (SDS) shows $\Delta h \propto c^{-1/3}$ scaling. Subsequently, stratification in liquid crystals films was attributed to the influence of structural contribution to disjoining pressure.[37, 64-68] Subsequently, starting in 1988, a series of papers by Nikolov, Wasan, Kralchevsky and coworkers[33, 35, 69-77] showed that films made with latex particle suspensions also stratify, and attributed stratification to confinement induced layering of micelles or latex particles. Stratification typically proceeds by nucleation and growth of one or more thinner, darker domains and the number of spontaneously formed domains and their thickness progressively decreases.[31, 33-36, 49-54, 59-62, 69, 78-83] Since disjoining pressure is defined as the free energy associated with thickness change,[27, 30, 31] it is well-accepted that the thickness-

dependent free energy functional is also oscillatory, and the coexisting thick-thin regions represent metastable states. Thermodynamically, such an oscillatory free energy functional ought to make the freestanding films susceptible to spinodal-like phase separation into thick and thin regions through the spontaneous growth of unstable thickness fluctuations, just as is observed in supported films that undergo spinodal dewetting.[1-26]

However, in addition to the lack of reports on the formation of spinodal-like thick-thin patterns, it must be emphasized that the characterization techniques like AFM (Atomic Force Microscopy) that allow thickness mapping in supported films[3-8, 18, 84] are unsuitable for thickness mapping in freestanding films. Likewise, the conventional interferometry-based thickness measurements in foam films measure an average thickness that is deduced from reflected light intensity from a 30-50 μm region.[30, 36, 49, 69] Such interferometry measurements lack the spatial resolution necessary for characterizing thickness variations in stratifying foam films. However, we recently showed that IDIOM (Interferometry Digital Imaging Optical Microscopy) protocols[50-52, 54] allow thickness mapping with exquisite spatial resolution (thickness ~ 1 nm, in plan < 1 μm). The IDIOM protocols rely on the use of a digital camera with its large array of photodiodes to measure the pixel-wise intensity variation, that yields highly spatially-resolved visualization of thickness variations with much better time resolution (< 1 ms).

In the present contribution, we utilize the IDIOM protocols to obtain the high resolution, thickness maps of spinodal-like, thick-thin regions in stratified micellar foam films. We find that spinodal structures appear only in studies carried out in vertical configuration and in experiments carried out in open cells implying that enhanced

drainage in vertical films, as well as evaporation effects help in driving spinodal stratification. In this report, we first contrast the thickness transitions in stratifying foam films in open and closed cells using horizontal foam films. Thereafter we visualize and analyze the spinodal stratification patterns in individual vertical films as well as three-dimensional foams, and we find that the thickness-dependent, oscillatory free energy results in nanoscopic hills and gullies as well as hierarchical layered structures. The discovery and analysis of spinodal stratification, and related discussion of the role of micellar interactions and thickness-dependent disjoining pressure, are expected to inspire new directions in research and applications targeting molecular engineering of foams.

MATERIALS AND METHODS

Aqueous surfactant solutions are formed at room temperature by dissolution sodium dodecyl sulfate (SDS) into a glycerol-water mixture. Glycerol (molecular weight of 92.1 Daltons, rpi, >99.0%) is used as received and is added with volume fraction ($\phi_{\text{glycerol}} = V_{\text{glycerol}} / V_{\text{solution}}$) below 10%. Even though the solution properties like surface tension and viscosity with <10% glycerol added are quite close to aqueous surfactant solutions, addition of glycerol is said to decrease the evaporative losses. A rectangular steel frame was used to form the thin foam films with $0.66\ \text{mm}$ thick square wire frame, with two horizontal and two vertical wires separated by 10 mm. The steel frame was extended with two wires and affixed to a steel column. Foam films were formed by moving the container filled with SDS solution in vertical direction with a motorized linear stage (Velmex XSlide) using a Velmex VXM-1 stepping motor controller, while keeping the frame stationary. The container was painted black to reduce any reflection from the surrounding walls and to allow for better imaging and cleaner images for

analysis. The schematic of the experimental setup is shown in Figure 2a. The film is illuminated with the white LED light source (Fiilex P360EX) with adjustable color temperature (set to 5100K for most experiments), and the changes in reflected light intensity are captured by using a high-speed, color FASTCAM Mini UX 100 camera with 12 bit RAW imaging capability, and suitable magnification optics. The thickness of the film is calculated from pixel-wise intensity by using interferometry equation, and relying on the high spatio-temporal resolution of IDIOM protocols[51], detailed elsewhere. The relation between interference intensity and thickness accounts for the phase shift contributed both by difference in the path length of light reflected from the two interfaces and the additional 180^0 phase difference due to reflection at the first air-liquid interface.

RESULTS AND DISCUSSION

Drainage of horizontal foam films: evidence for stratification

Aqueous 70 mM SDS solutions (containing 8 vol.% glycerol) display two most notable features of stratification as shown in Figure 1: (a) the stepwise decrease in thinning observed in the plot of average thickness *vs.* time data and (b) the coexistence of thick-thin regions that appear as iso-intensity gray regions in snapshots. The experiments were carried out in a Scheludko cell, such that the foam film drainage emulates the drainage from a horizontal foam film. Since the experiments are carried out for SDS concentrations well above the CMC= 8.2 mM, we observe evidence for stratification, including the spontaneous formation of thick-thin regions by nucleation and growth of thinner, darker domains. Unlike most of the previous studies that utilize a closed system to minimize evaporation effects,[31, 33-36, 42, 45, 49-54, 59, 69, 78, 79, 81-83] here we compare the

drainage kinetics in an open and closed system. In the open system, as the cover of the cell is removed, the foam film has the possibility of enhanced drainage due to evaporation as well as flows driven by ambient air currents.[45, 85] The comparison of the two datasets reveals the following salient features. The number of layers during stratification is not affected by the evaporation; both open and closed systems exhibit five layers. However, the rate of drainage is faster in the open cell compared to the closed one. The step size Δh in a closed system is 11.3 nm (except the last layer transition from h_1 to h_0), however, in an open system, the step size decreases continuously during each transition, such as $h_3 - h_2 = 10$ nm, $h_2 - h_1 = 9.2$ nm and $h_1 - h_0 = 6$ nm.

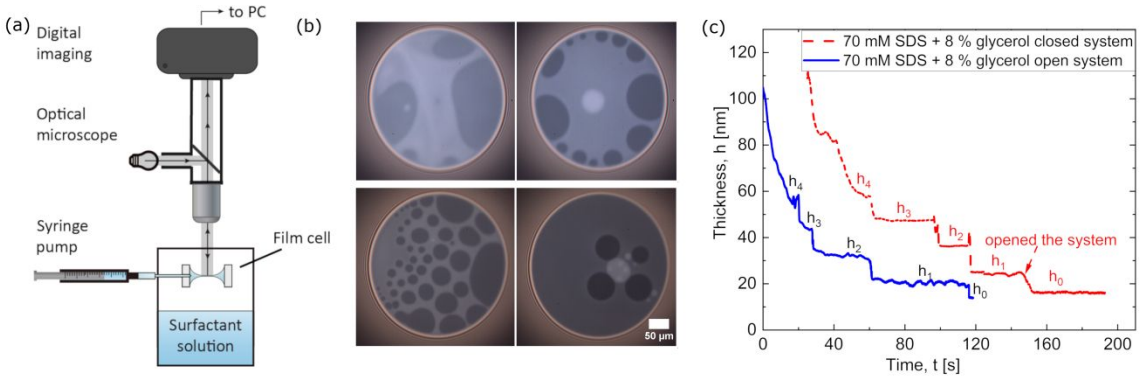

Figure 1 Drainage in horizontal foam films in an open system contrasted with behavior in a closed system. (a) Schematic of the IDIOM (interferometry digital imaging optical microscopy) set-up. A high speed camera is used for capturing reflected light images from a stratifying, single foam film, formed within a 1-2 mm pore within a glass tube (Scheludko cell), as shown. (b) Drainage and stratification in aqueous 70 mM SDS (and 8 vol% glycerol) foam films in horizontal foam films in a closed (first row) and open system (second row). The scale bar corresponds to 50 µm. (c) Thickness evolution with time for an open and closed system is calculated and plotted for 25 µm a side square region. In the closed system, the thickness transition appear progressively, but the last thickness transition from h_1 to h_0 is achieved by opening the cover of the container.

Most of the published experimental studies, (including our previous papers),[49-51, 54, 75, 86-90], utilize a closed cell for measurement of the step-size and stratification dynamics, though several papers[38, 73, 91, 92] do mention that the experimental cell was

opened for few seconds to trigger the stepwise transition(s) in the last stage or two of stratification. Our current results suggest that the evaporation leads to lower step-size, which is correlated with higher effective surfactant concentration.[38, 53] The formation and expansion of nearly circular domains, the decrease in the relative number of such domains formed as film thickness decreases or concentration increases, and the quantized difference in thickness of flat regions, all suggest that stratification as visualized in Figure 1 represents the progressive descent of the system from one metastable state to the next, each with lower energy well, each requiring a larger activation energy. Next we investigate how these transitions change when experiments are repeated using vertical films.

Drainage of vertical foam films: evidence for spinodal stratification

Freshly formed foam films exhibit iridescent colors under white light illumination associated with the thickness-dependent constructive or destructive interference between rays reflected from the two liquid-air interfaces. The simplest experiment carried out using the set-up shown in Figure 2a typically yield multicolored, iridescent films. The montage in Figure 2b emulates countless experiments carried out in a closed cell that yield films that display nearly uniform interference color bands at a given height, and color changes in the vertical direction due to height-dependent thickness variations detailed in many studies.[45, 93-95] The appearance of soapy shades of gray in the later stages is associated with drainage to thicknesses below 100 nm, and nearly black films are observed below 20 nm. The image sequence included in Figure 2b shows snapshots for a foam film containing 70mM SDS in glycerol-water mixture (8 vol. % glycerol) undergoing free drainage in a closed cell, and Figure 2c shows the snapshots that

correspond to an open system. The open cell shows the existence and appearance of remarkably distinct network-like patterns shown in Figure 2c. Such patterns are visible neither in experiments carried out using the horizontal configuration (in Scheludko cell) described in Figure 1 (both open or closed cells) nor in experiments that visualize and analyze drainage in vertical foam films in a closed cell (Figure 2b).

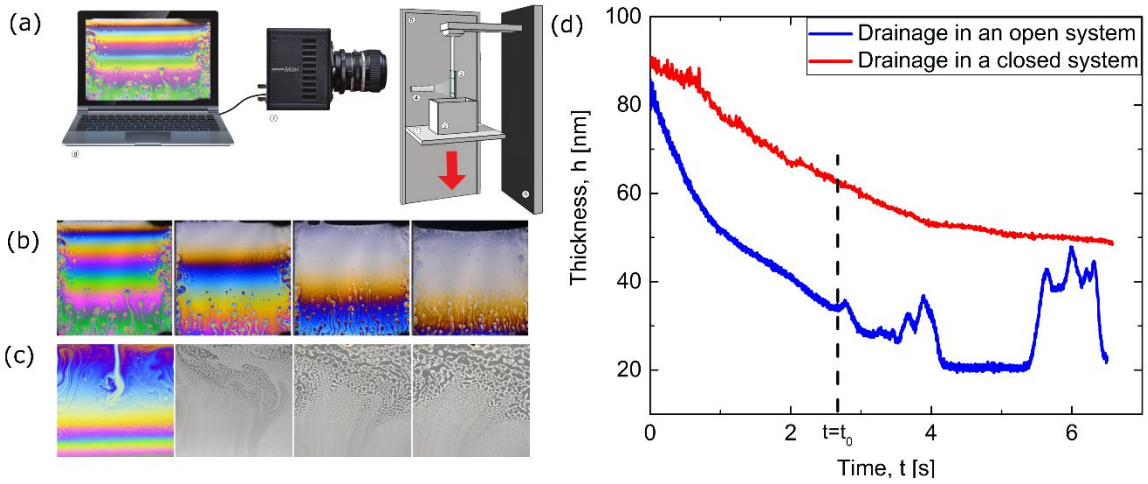

Figure 2. Drainage of vertical foam films in closed *vs.* open cells. (a) Schematic of the experimental setup used for visualizing and characterizing spinodal stratification. The frame, illumination and camera are kept fixed. The frame is dipped into a soap solution placed within a container, and soap film gets created when the container placed on a motion stage is moved down. (b) Snapshots show drainage of a vertical foam film in a closed setup (c_{SDS} = 70 mM, $\phi_{glycerol}$ =8%). The vibrant interference colors arise in for $h > 100$ nm and gray regions correspond to h <100 nm. (c) Bi-continuous network structure with distinct gray scale intensity regions forms due to spinodal stratification in experiments carried out in an open cell. (d) Thickness evolution over time data for the open and closed system acquired using the IDIOM protocols reveal that drainage in a closed system is slower and thickness decreases monotonically. The film thickness decreases at a much faster rate due to evaporation and possibly influence of air currents, and the measured thickness shows dramatic fluctuations after the onset of spinodal stratification.

To contrast the drainage kinetics between the open and closed cell, we first compare the average thickness as a function of time at the center of the film by utilizing interference intensity from a 25 μm side square as shown in Figure 2d. Unlike stratified horizontal foam films, the average thickness at a spot within vertical films exhibits a

monotonic decrease with time. The drainage kinetics for a closed system is noticeably slower than that observed for the open system. Thus, a rapid reduction in thickness in an open system induces the film thickness to reach an unstable state and results in the emergence of a polygonal, bicontinuous, network-like morphology in the freely draining vertical foam film. The dotted line is chosen to represent the initial time where $t = t_0$ after which the thickness fluctuations begin to increase (see Figure 2d). We find that spinodal patterns only appear for concentrations above 60 mM (see montages included in Figure S1 in supplementary document online).

Mapping nanoscopic thickness variations due to spinodal stratification using IDIOM protocols

The thickness variations associated with the evolving pattern are analyzed using the IDIOM protocols that convert the pixel-wise reflected light intensity to a highly spatially resolved measure of thickness. Such AFM-like thickness maps of vertical foam films have never been constructed or reported before; we display the maps in Figure 3, for demonstrating the non-flat landscape associated with network patterns observed in the gray scale images. The thickness evolution associated with spinodal stratification is examined in Figure 3, by focusing on a 1.2 mm a side region. The color bar on the right shows the thickness range in nanometers, while the horizontal scale is in 1- 1200 μm, thus implying all the features are relatively flat or small slope approximation applies. The film is driven to spontaneously separate into the regions of distinct gray scale iso-intensity, and for each image, the corresponding thickness map is reconstructed using the interferometry formula with intensity measured from images acquired in the unfiltered, unprocessed RAW format. While the typical size of the plane-parallel film in a

Schedulko cell is 1-2 mm, the vertical foam film experiments utilize a wire frame that allows investigation of a 10 mm by 10 mm freestanding film. The size of the film is chosen to be large enough such that the pattern formation described here is not directly influenced by marginal regeneration,[43, 45, 96, 97] a term used to refer to the highly complex flows that arise in the margins, where the thinner liquid film connects to the curved, thicker Plateau border region.

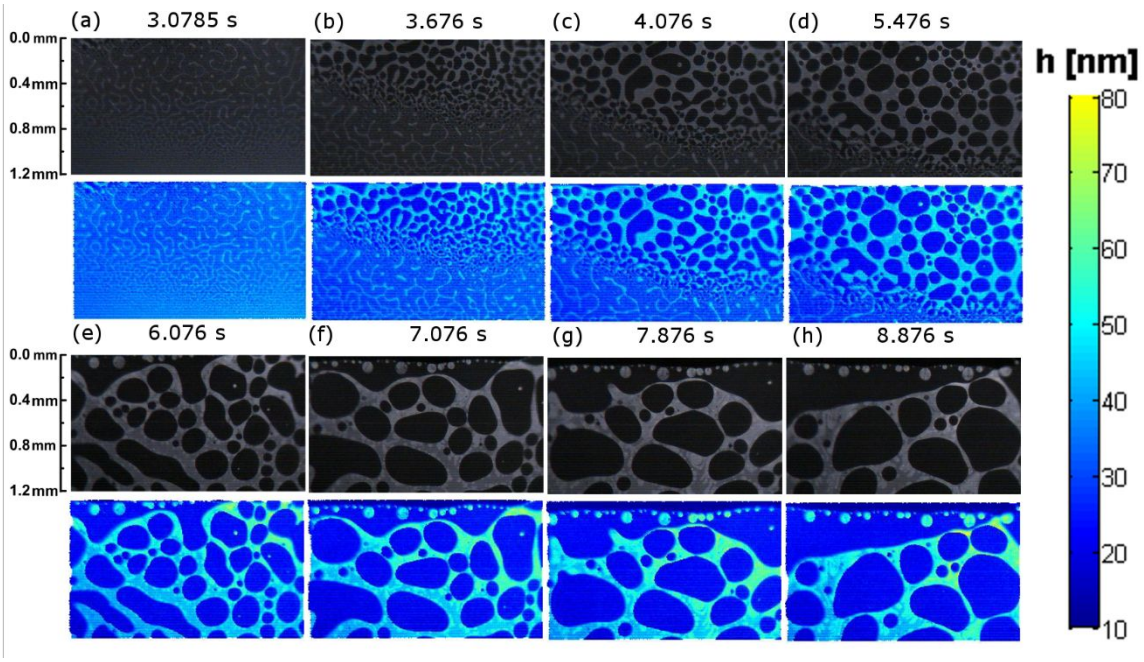

Figure 3. Thickness map for spinodal stratification obtained by IDIOM protocols in foam films made with 70 mM SDS + 8 vol.% glycerol. Snapshots show the evolution of spinodal stratification in the foam film. Bright and dark regions indicate coexistence of thick-thin regions in the bicontinuous network structures. The thickness map of the film with distinct colors shows that the film separates into different thickness. The thickness of the film varies between 10 and 80 nm, while the in-plane scale bar shows domains are 1-1200 μm.

Experiments carried out at a slightly higher SDS concentration (80 mM), shown in Figure 4, share the network-like pattern structure corresponding to the nanoscopic hills and gullies revealed in thickness maps. On a closer glance, the morphology evolution reveals the coexistence of multiple steps (see Figure 4d-f) within the thicker domains,

implying sequential stratification events can take place. Furthermore, in contrast with Figure 3, we intentionally show a larger section of the film undergoing spinodal stratification in Figure 4 to highlight the thickness-dependent variation in morphology evolution in vertical direction, for vertical foam film is known to get thinner as a function of height. Therefore, the spinodal structure first appears within the lower half of the images at a later time instant, and the same snapshots show early and late stage of morphological evolution. The different stages in morphology evolution are discussed in a subsequent section, after examining the mechanism that drives spinodal stratification.

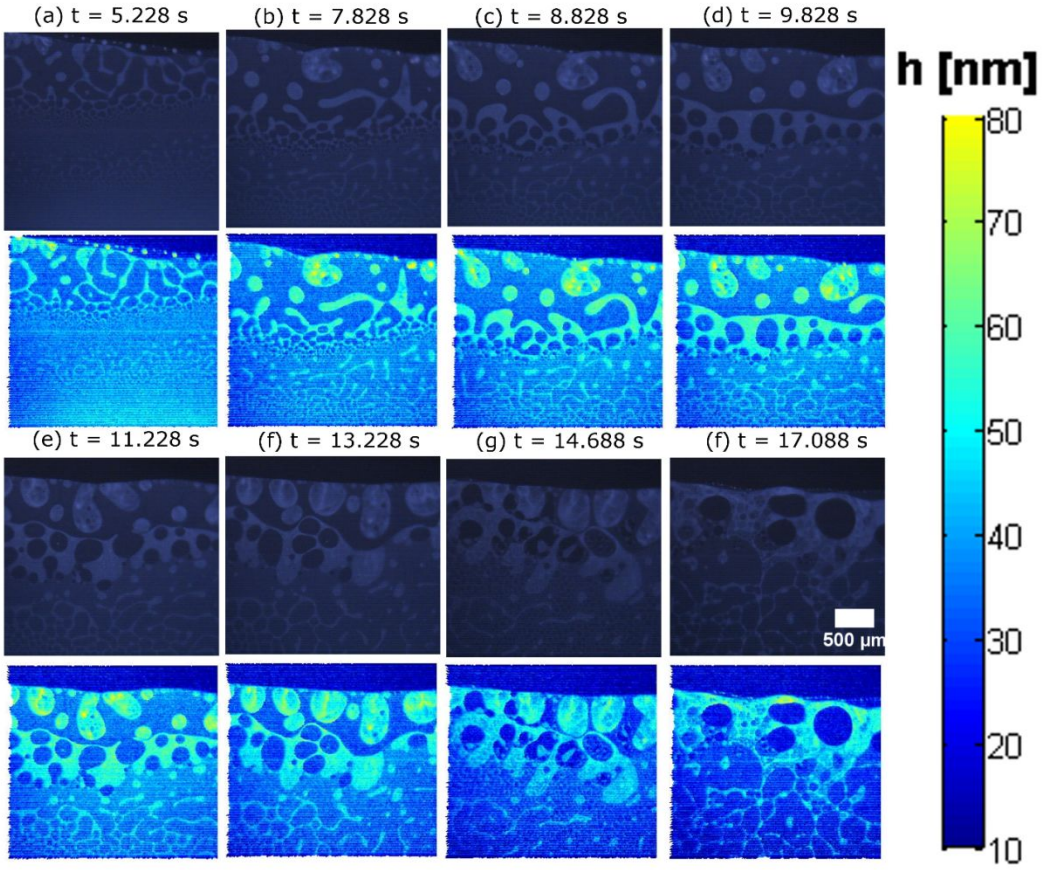

Figure 4. Spinodal stratification and the corresponding thickness maps for vertical foam film formed with aqueous SDS solution (80 mM SDS with 8 vol.% glycerol). Bright and dark regions indicate coexistence of thick-thin regions for the spinodal stratification. The thickness of the film varies between 10 to 80 nm, while in-plane scale bar shows domains are 1-1200 μm.

Oscillatory free energy drives spinodal stratification in foam films

The theoretical analysis and arguments made by Vrij using a thickness-dependent free energy functional form the basis of several theoretical and experimental studies in the context of spinodal dewetting studies.[1, 5-8, 17, 84] In unstable thin films, thickness fluctuations play a role analogous to the role played by composition fluctuations in unstable binary mixtures. Recently Zhang and Sharma[54, 88] utilized a nonlinear thin film equation model $\partial_t h + \nabla.\left[M\nabla P \right] = 0$ to model nanoridge growth and shape, as well as nanoridge-to-mesa instability in stratifying micellar films. The partial differential equation for thickness h includes the effective mobility term $M = h^3/3\eta$ that is determined by the fluid viscosity, η and the equation explicitly accounts for the total pressure $P = \sigma \mathrm{K} + \Pi(h)$ contributed by: (a) Laplace pressure arising from the local surface curvature, K and the bulk surface tension, σ and (b) disjoining pressure, $\Pi(h)$ contributed primarily by the supramolecular oscillatory surface force contribution. The nonlinear thin film equation that captures the complex spatio-temporal evolution of nanoscopic thickness variations and transitions in stratifying films (in closed system) can be considered to be a manifestation of dissipation dynamics[8, 17] with the form $\partial_t \phi + \nabla.\left[M\nabla(\delta F/\delta\phi) \right] = 0$. Thus, the thin films model treats thickness as the conserved order parameter $\phi(r,t)$ with evolution governed by the surface energy functional $F(\phi)$ (a Lyapunov parameter in this case), and thus belongs to the same class of problems as the Cahn-Hillard model for phase separation in which case energy functional is composition based.[1, 8] In Figure 5, we contrast the free energy functional, and its first and second order derivative with respect to the respective order parameter

(composition or height) as obtained for compositional phase separation in binary mixtures and thickness-based spinodal stratification in stratifying films.

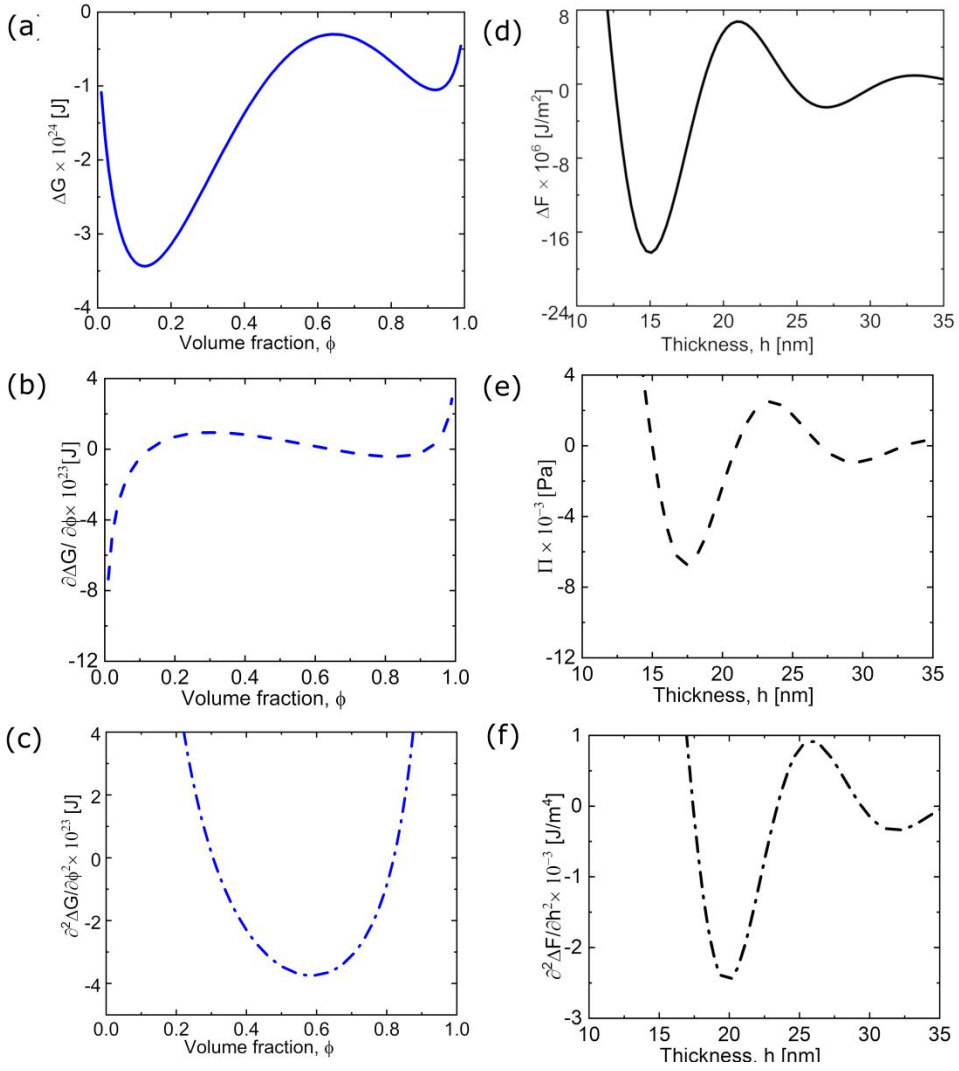

Figure 5. Comparison between spinodal decomposition in binary mixtures, and spinodal stratification in foam films. (a) Composition-dependent free energy of mixing is constructed from Flory-Huggins equation for polymer solution, and (b) – (c) respectively show the first and the second derivative of free energy of mixing. (d) Surface free energy of the micellar foam films is calculated for 70 mM SDS foam films, using (e) the supramolecular oscillatory structural force contribution to disjoining pressure. The second derivative of the free energy (f) is then calculated and shows the potential for hierarchical spinodal stratification, due to existence of multiple extrema in free energy term as shown in (a).

In Figure 5a, a composition-dependent free energy curve calculated by using the Flory- Huggins model that accounts for both entropic and enthalpic changes on mixing is shown. The single curve is shown for a temperature for which the binary mixture with intermediate compositions is susceptible phase separation by spinodal decomposition. The phase space for a binary mixture is extracted from a family of such curves that can be drawn by accounting for temperature-dependent change in interactions. It is well-established experimentally and theoretically that a binary mixture that is unstable to composition fluctuations phase separates by forming bicontinuous structures due to spinodal decomposition[98-101] if the second derivative of the free energy with respect to composition is negative, i.e. $\partial^2 \Delta G / \partial \phi^2 < 0$. Such compositional phase separation is often driven by a temperature jump into the thermodynamically unstable state, and the unstable range of concentrations can be identified using Figures 5a-c. Both experimental and theoretical studies on phase separation of simple liquids and polymer mixtures show that the quench depth and interaction parameter determine the structure and dynamics of resulting patterns.[2, 99-102]

In contrast, the thickness-dependent surface energy functional, shown in Figure 5d, for thin film case is computed using $\Delta F = \int \Pi dh$ by utilizing a phenomenological expression for disjoining pressure contributed by supramolecular oscillatory structural forces (plotted in Figure 5e) we developed recently,[53] and and summarized here. The phenomenological expression includes a pre-factor that depends on thermal energy ($k_B T$), the number density of the micelles ($\rho = (c - cmc) N_A \big/ N_{agg}$), and a compressibility factor derived by Carnahan and Starling for hard spheres[103].

$$\Pi_{os} = \frac{(c - cmc)N_A}{N_{agg}} f(\varphi) k_B T \cos(\frac{2\pi h}{\Delta h}) \exp[((\frac{d}{\Delta h})^3 - \frac{h}{\Delta h}) g(\varphi)] \quad (1a)$$

$$f(\varphi) = \frac{\left(1 + \varphi + \varphi^2 - \varphi^3\right)}{(1-\varphi)^3}; \; g\left(\varphi\right) = \frac{\sqrt{2/3} + a_1 \Delta\varphi + a_2 (\Delta\varphi)^2}{\left(b_1 / \Delta\varphi\right) - b_2} \quad (1b)$$

Here, the pre-factor explicitly shows the dependence on surfactant concentration, critical micelle concentration, aggregation number, temperature, and the effective volume fraction, φ of the micelles that is defined as $\varphi = \rho\pi d^3/6$ using an effective micelle diameter $d = 2(l_{SDS} + \kappa^{-1})$ computed by adding the characteristic size of counter-ion atmosphere or Debye length, κ^{-1} to the micelle size, $l_{SDS} = 2.3$ nm determined from the length of SDS molecules.[92] we used. The values of parameters $\Delta\varphi = \pi/3\sqrt{2} - \varphi$ and the values for $a_1 = 0.24, a_2 = 0.63, b_1 = 0.49, b_2 = 0.42$ are based on the formulas and values determined by Kralchevsky and Denkov[74]. The plot in Figure 5f shows the corresponding second derivative of free energy functional, and here we find that the presence of supramolecular oscillatory structural forces makes the thin films susceptible for phase separation into spinodal-like thick/thin regions for multiple values of thickness. Thus unlike spinodal dewetting that results in creation of two coexisting thick–thin regions, spinodal stratification can be expected to show hierarchical coexisting thick-thin regions. Even though compositional phase separation *via* spinodal decomposition is usually triggered by temperature jump, we posit and find that the unstable region in stratifying films is accomplished primarily through a thickness-jump, as discussed next.

Evolution of spinodal stratification in free-standing foam films

Unlike horizontal films, the thickness variation and transitions in vertical foam films are harder to analyze due to additional flow contributions from (a) the influence of buoyancy and gravity that cause lighter, thinner regions to rise and heavier, thicker regions to sink in the vertical direction,[45, 104] (b) marginal regeneration near the Plateau borders[43, 45, 96, 97, 105, 106] (mechanism is still under debate) and (c) the influence of the ambient air currents in an open cell. In Figure 6, we show the gray scale intensity images of a region of interest by following and tracking a constant size square area (with 0.77 mm side). As the evolving spinodal stratification patterns are advected by flow, we include spatial coordinates to visualize the relative displacement of the region of interest. In each micrograph from Figure 6 (a) - (d), the y-axis represents the vertical position of the square region, and the x-axis represents the horizontal position (the film itself is 10 mm size). For each selected region on the left in Figure 6, the corresponding variation in film thickness is plotted on the right as a line profile. The thickness as a function of distance is defined in the moving coordinate to make the comparison shown in Figure 6 (e)-(h). The increase in the amplitude of thickness variation as a function of time, as well as the change in wavelength over which thickness variations manifest themselves can be directly read from these graphs. The line profiles for thickness variation look quite similar to the concentration-distance evolution profiles of spinodal decomposition in the binary mixture, observed and reported Hashimoto *et al.*[102] (see their Figure 11), Bates *et al.,*[99] among others. The film spontaneously starts to develop sinusoidal capillary waves as shown in Figure 6, signaling the onset of instability.

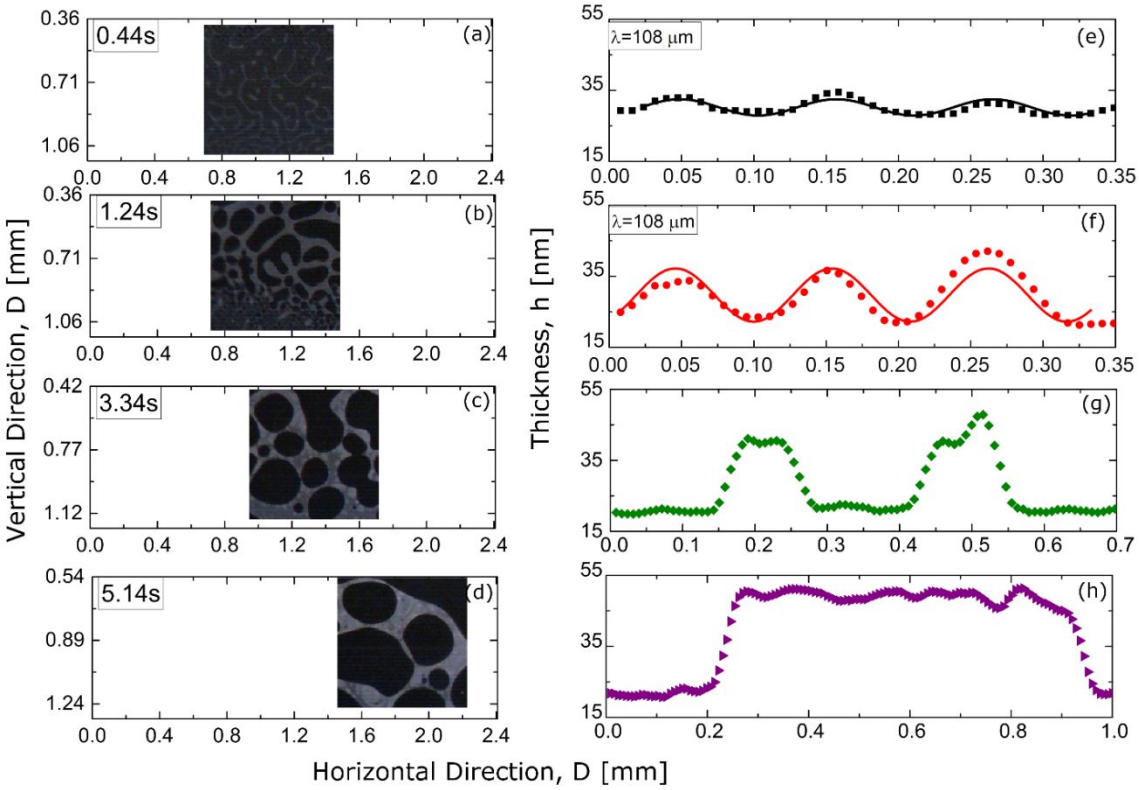

Figure 6. The thickness evolution during spinodal stratification in the foam films. (a-d) Regions with similar thickness are observed to have similar gray scale intensity in reflected light microscopy images. As the spinodally stratifying regions are advected by the complex flows within the vertical foam film, change in thickness is determined over a particular region that is tracked over time. The micrographs show the movement of the pattern in horizontal and vertical direction, and also the evolution of the pattern. (e-h) Thickness is measured over a same horizontal line for the micrographs presented in (a-d). Thickness profiles show three different stages of spinodal stratification including the initial regime associated with growth of thickness fluctuations, an intermediate regime with constant wavelength and thickness saturation and coarsening in the late regime.

The spatio-temporal variation in thickness is captured well by the form $h - h_0 = H \sin\left(2\pi x / \lambda\right)\exp\left(\alpha t\right)$ for 70 mM SDS solutions (also see supplementary information for similar analysis for 80 mM case, and plot of peak height *vs*. time), and the values obtained are $h_0 = 30$ nm, $\lambda = 108$ μm, $\alpha = 0.25$ s^{-1} and $H = 3$ nm respectively. Thereafter the peak amplitude of the thickness variation progressively grows, even though the wavelength stays the same in Figure 6e-f, and this intermediate

regime of growth is similar to similar change in composition observed in phase separation studies. Subsequently the thickness of the film saturates at maximum values (see Figure 6g-h), and the pattern continues to coarsen, leading to an increase in the wavelength of the instability and coalescence between thinner regions. Since such features are present only in open films, evidently the faster drainage in an open cell, pushes the system into the unstable thickness that is susceptible to spinodal stratification.

The criteria for instability can be obtained by analyzing the thin film equation and accounting for the thickness-dependent the free energy of thin films per unit area. Vrij[1] argued that thickness fluctuations grow if their wavelength $\Lambda > \Lambda_c$ exceeds a critical wavelength $\Lambda_c = \left[-2\pi^2\sigma / \left(d^2\Delta F / dh^2 \right)_0 \right]^{1/2}$ that depends on the value of surface tension, σ and intermolecular and surface forces that contribute to the free energy of thin films per unit area. The fluctuations with wavelength $\Lambda < \Lambda_c$ are dampened, and the most unstable mode is typically manifested. The critical wavelength is similar to the critical lengthscale postulated by Scheludko.[30] To evaluate this critical wavelength for the stratifying micellar foam films requires the assumption that the kinetics of spinodal stratification involve the role supermolecular structure forces (and any additional effect of evaporation). If we can make a simple estimate, following the arguments for effective value of $\left(d^2\Delta F / dh^2 \right)_0 = d\Pi / dh \approx 4P_c / \Delta h$ as decribed by Zhang and Sharma,[52] the wavelength estimate for the SDS foam film comes out to be 50 micron, which is within a factor of two of the observed wavelength. The dominant growth rate, $\alpha \approx \left(h_0^3 / 24\eta\gamma \right)\left(\partial\Pi / \partial h \right)^2$ can be estimated to be 0.3 s^{-1} and agrees well with the observed

value of 0.25 s^{-1} obtained from data shown in Figure 6. In the late stage, the contact angle between thin regions (gullies) and thicker regions (hills) approaches a constant value, quite reminiscent of the shape and contact angles of nanoridges observed around the expanding domains in stratifying horizontal micellar foam films.[52] We posit that the coaresening dynamics, are governed by the velocity scale set by the ratio of change in surface energy at the foothill to the viscosity of the micellar solution, in analogy with constant velocity mode (v ~ 50 μm/s) observed in the late stages in domain expansion dynamics.[50-52, 54] However, the discussion of oscillatory free energy functional and the phase diagram outlined in Figure 5 exclude evaporation effects that can change both the proportion of glycerol present in the fluid and the absolute concentration of surfactant within the fluid. In analogy with the related experimental and theoretical studies on spinodal dewetting of volatile films, the inclusion of evaporation effects will lead to non-conserved order parameter, need for comparison between additives of different volatility, and closer examination of how supramolecular structural forces change with composition; related experimental studies are underway.

The supramolecular oscillatory structural forces are oscillatory and therefore it is expected that spinodal stratification can show a hierarchical step-wise structure, as discussed in the previous section in connection with the features observed in Figure 5d-f. Likewise, it seems plausible that the spinodal stratification mechanism would manifest itself in actual three-dimensional foams, and in many applications, foams are indeed in an open system. Furthermore, it can be anticipated that the features appearing in each vertical film would display nuanced differences corresponding to the difference in local drainage rate, evaporation rate, film orientation, and capillary pressure that itself depends

on film size. Figure 7a-b show the thickness map of the coexistence of multiple layers of spinodal stratification. Close examination of the thickness map shows that three different thicknesses exist simultaneously. Similarly, simultaneous appearance of nucleation and growth mechanism and spinodal stratification can also be seen in foam films as shown in Figure 7b. Formation and evolution of these intermediate layers are quite fast (in milliseconds), and one reason why we are able to visualize these is the use of a color high-speed camera. The presence of oscillations in free energy of micellar foam films allows multiple windows of thicknesses where the spinodal parameters are negative. In contrast, there is only one hump or oscillation in the free energy functional used in describing concentration-dependent spinodal decomposition in binary mixtures and thickness variations associated with spinodal dewetting.

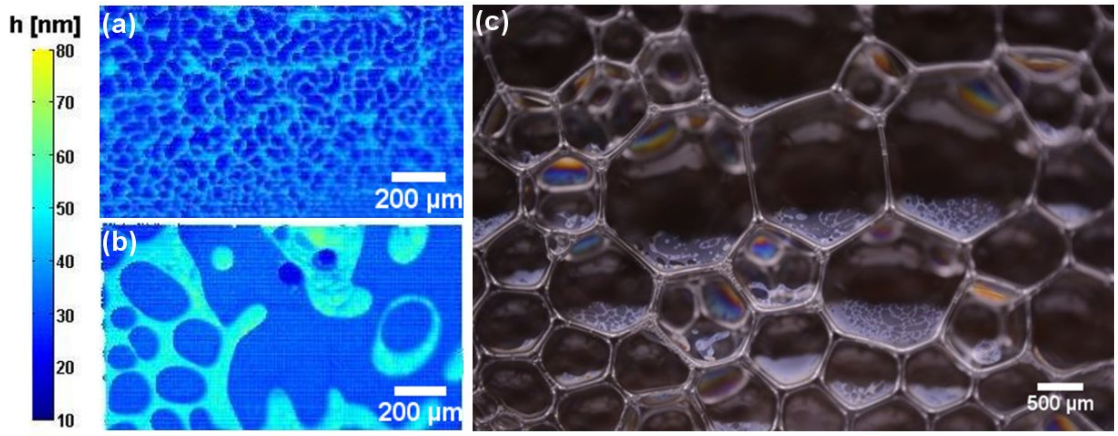

Figure 7. Multistage spinodal stratification in a single vertical foam films and evidence of spinodal stratification in 3D foam (a) Thickness map of formation of multiple layers of spinodal stratification in one instance in the film due to non-monotonic oscillatory free energy. (b) Thickness map of formation of spinodal stratification and nucleation of thinner domains in the film at the same time. (c) Spinodal stratification in a three-dimensional foam, showing the single film experiments provide insights into rupture process that can influence the stability and lifetime of foams relevant in industry and daily life.

Lastly, in Figure 7c we show spinodal stratification in foams made with aqueous solutions of SDS (70 mM SDS, and 8 vol. % glycerol). Patterns formed by spinodal stratification are simultaneously visible in many different films in this three dimensional foam. The image highlights the importance of investigations into spinodal stratification as a mechanism for film drainage and rupture, and also shows that the pattern formation observed in single vertical foam films is representative of the thickness variations and transitions in real foams. Even though the Laplace pressure acting in each film depends on the film size, the effect of gravity depends on the film alignment, and flows driven by gravity/buoyancy as well as evaporation vary from one film to another, we find that the spinodal stratification patterns show characteristics similar to the patterns observed in single vertical films and analyzed in Figures 2-4, 6 and 8.

The spatiotemporal variation in thickness of films undergoing spinodal stratification, and the emergence of nanoscopic hills and gullies can be visualized more easily in thickness maps shown using an oblique perspective, as shown in Figure 8. The observed thickness variation between hills and gullies ranges from thickness $h_h \approx 35\,\text{nm}$ to $h_g \approx 20\,\text{nm}$. In the late stages (see Figure 8c), the thinner, darker domains become more circular. Without the use of IDIOM protocols to resolve the entire pattern formation process, such late stage patterns can be construed to be a result of nucleation and growth of a large number of domains. The topographical color maps in Figure 8d-f show that the emerging structures grow, merge, and coalesce and also get advected by the flows within the soap film throughout the different stages of the spinodal stratification process. The drainage via stratification eventually leads to film rupture, and understanding the topological transitions thus can help in designing less or more stable foams.

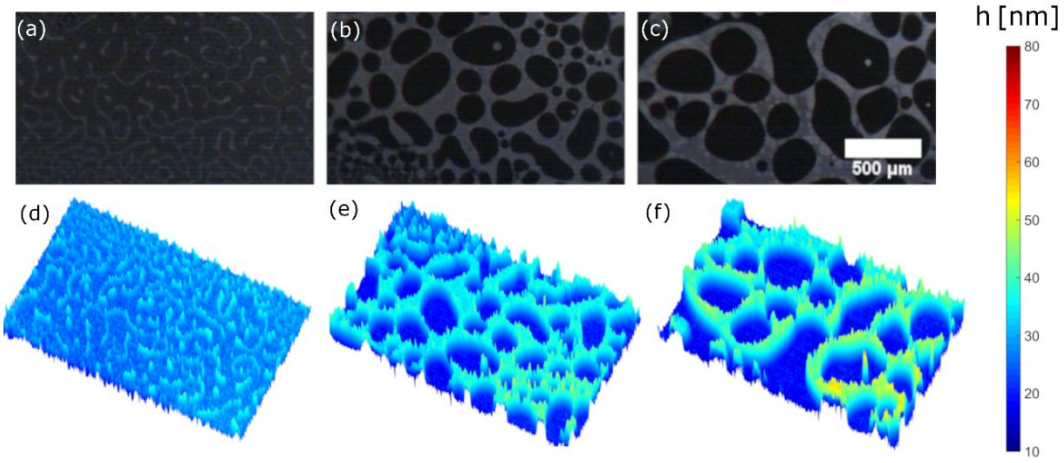

Figure 8. 3D view of thickness map for spinodal stratification patterns. (a)-(c) The iso-intensity gray scale regions correspond to same thickness regions. The network-like structure of patterns, and coarsening over time can be visualized in unprocessed images. (d)-(f) IDIOM protocols allow a reconstruction of a 3D thickness map, and the oblique view allows the visualization of hills and gullies in their different stages of evolution. The scale bar corresponds to 500 µm .

CONCLUSIONS

To summarize, we report the discovery, visualization and analysis of spinodal stratification, i.e. network-like pattern of thick-thin regions or "hills and gullies" in ultrathin free-standing micellar foam films. In 1966, Vrij predicted the possibility of the formation of spinodal patterns in both freestanding and supported thin films by accounting for the role of van der Waals forces and electrostatic double layer forces (together refered to as DLVO forces) in dictating the free energy of the thin films. However, Vrij never considered the case of micellar films and the influence of non-DLVO forces. Though the observation of spinodal dewetting in thin films of metals and polymers deposited on substrates followed Vrij's mechanism, in the last fifty one years (and datasets recorded over centuries!), there seem to be no reports of spinodal patterns in foam films.

We find spinodal stratification in ultrathin free-standing micellar foam films can be observed in both single foam film as well as in a three-dimensional foam. The morphology and evolution of the pattern are qualitatively similar to the different stages of fluctuation growth, intermediate growth at constant wavelength, and late stage growth by coarsening as is observed in the spinodal decomposition from in binary mixture that leads to the creation of compositionally-distinct regions. We contrast the composition-dependent free energy calculated using the Flory-Huggins theory for binary mixtures with the corresponding plot for the thickness-dependent free energy functional, evaluated by integrating disjoining pressure expression. In both cases, the spinodal patterns appear if the initial composition or thickness corresponds to a higher free energy for the system, than possible with the segregated regions formed after spinodal decomposition and spinodal stratification respectively.

Historically, stratification in micellar foam films is associated with nucleation and growth of thinner domains that grow at the expense of surrounding thicker films and it is well-established that the stepwise thinning is manifestation of transition from one metastable thickness to the next. More recently, we have examined the formation of thicker white spots, that we term mesas as they are pancake like structures, and we postulate that these structures are also sculpted by the supramolecular oscillatory structural forces through a nucleation and growth mechanism. The observation of spinodal stratification appears to complete the thickness-dependent phase diagram of micellar foam films, though a more quantitative analysis will be needed to account for the critical role played by evaporation. The thickness maps and localized thickness evolution

data show that the faster drainage in evaporative system forces the films into reach to an highly unstable thickness.

We anticipate the present study will lead to further investigation into spinodal stratification, establishing it as mechanism than can determine and control foam stability and lifetime. We find that carrying out the experiments in an open cell was critical to creation and observation of the unexpected spinodal-like pattern formation. Furthermore, we recognize that the use of high-speed imaging allowed us to capture these transient patterns in both single vertical foam films and in bulk foam, but in spite of hundreds of trials and repeats we have not yet observed the spinodal patterns in horizontal foam films even for an open system. The present investigation also highlights the success and significance of the IDIOM protocols we developed, for the use of IDIOM protocols provide thickness maps with exquisite spatio-temporal resolution, enabling visualization of nanoscopic hills, gullies and valleys, as well as hierarchical stratified structures. Experimental studies on the visualization and analysis of spinodal stratification presented here are also critical steps towards an understanding of the role of supramolecular oscillatory structural forces in driving flows, instabilities and controlling the lifetime of micellar foam films, and advance the ability for molecular engineering of foams with desired lifetime and stability.

ACKNOWLEDGEMENTS

VS would like to acknowledge funding from National Science Foundation (NSF CBET 1806011) and the initial funding support by the College of Engineering and the Department of Chemical Engineering at University of Illinois at Chicago. VS also acknowledges funding for his Mentored Professional Development Program for Future Chemical Engineers at UIC that helped in motivating and funding a former undergraduate researcher (EW) for carrying out experiments included in this article. VS thanks Cynthia Jamieson, UIC for close reading of the manuscript and acknowledges students in ODES-

lab insightful questions and comments. SY also acknowledges the Chemistry department at UIC for funding her as a teaching assistant.

REFERENCES

1. A. Vrij, *Discuss. Faraday Soc.*, 1966, 23-33.
2. J. W. Cahn, *J. Chem. Phys.*, 1965, **42**, 93-99.
3. R. Xie, A. Karim, J. F. Douglas, C. C. Han and R. A. Weiss, *Phys. Rev. Lett.*, 1998, **81**, 1251.
4. S. Herminghaus, K. Jacobs, K. Mecke, J. Bischof, A. Fery, M. Ibn-Elhaj and S. Schlagowski, *Science*, 1998, **282**, 916-919.
5. G. Reiter, S. Al Akhrass, M. Hamieh, P. Damman, S. Gabriele, T. Vilmin and E. Raphaël, *European Physical Journal-Special Topics*, 2009, **166**, 165-172.
6. R. Blossey, *Thin Liquid Films: Dewetting and Polymer Flow*, Springer, 2012.
7. R. Mukherjee and A. Sharma, *Soft Matter*, 2015, **11**, 8717-8740.
8. S. Kalliadasis and U. Thiele, *Thin Films of Soft Matter*, SpringerWien NewYork, 2007.
9. J. K. Bal, T. Beuvier, A. B. Unni, E. A. Chavez Panduro, G. Vignaud, N. Delorme, M. S. Chebil, Y. Grohens and A. Gibaud, *ACS nano*, 2015, **9**, 8184-8193.
10. J. Chen, S. Qin, X. Wu, Chu and P. K, *ACS Nano*, 2015, **10**, 832-838.
11. F. Ferrarese Lupi, T. J. Giammaria, A. Miti, G. Zuccheri, S. Carignano, K. Sparnacci, G. Seguini, N. De Leo, L. Boarino and M. Perego, *ACS Nano*, 2018, **12**, 7076-7085.
12. R. Mukherjee, S. Das, A. Das, S. K. Sharma, A. K. Raychaudhuri and A. Sharma, *ACS Nano*, 2010, **4**, 3709-3724.
13. Y.-J. Oh, J.-H. Kim, C. V. Thompson and C. A. Ross, *Nanoscale*, 2013, **5**, 401-407.
14. P. Cao, P. Bai, A. A. Omrani, Y. Xiao, K. L. Meaker, H. Z. Tsai, A. Yan, H. S. Jung, R. Khajeh, G. F. Rodgers, Y. Kim, A. S. Aikawa, M. A. Kolaczkowski, Y. Liu, A. Zettl, K. Xu, M. F. Crommie and T. Xu, *Adv. Mater.*, 2017, **29**, 1701536.
15. R. Katsumata, R. Limary, Y. Zhang, B. C. Popere, A. T. Heitsch, M. Li, P. Trefonas and R. A. Segalman, *Chem. Mater.*, 2018, **30**, 5285-5292.
16. Y. Vaynzof, D. Kabra, L. Zhao, L. L. Chua, U. Steiner and R. H. Friend, *Acs Nano*, 2010, **5**, 329-336.
17. U. Thiele, *Colloids and Surfaces A: Physicochemical and Engineering Aspects*, 2018, **553**, 487-495.
18. A. Sharma and G. Reiter, *J. Colloid Interface Sci.*, 1996, **178**, 383-399.
19. A. Karim, J. F. Douglas, B. P. Lee, S. C. Glotzer, J. A. Rogers, R. J. Jackman, E. J. Amis and G. M. Whitesides, *Phys. Rev. E.*, 1998, **57**, R6273.
20. A. M. Higgins and R. A. L. Jones, *Nature*, 2000, **404**, 476.
21. R. Seemann, S. Herminghaus, C. Neto, S. Schlagowski, D. Podzimek, R. Konrad, H. Mantz and K. Jacobs, *J. Phys.: Condens. Matter*, 2005, **17**, S267.
22. A. A. Pahlavan, L. Cueto-Felgueroso, A. E. Hosoi, G. H. McKinley and R. Juanes, *J. Fluid Mech.*, 2018, **845**, 642-681.
23. P. G. de Gennes, F. Brochard-Wyart and D. Quere, *Capillarity and wetting phenomena: drops, bubbles, pearls, waves*, Springer, 2003.

24. M. Lessel, J. D. McGraw, O. Bäumchen and K. Jacobs, *Soft Matter*, 2017, **13**, 4756-4760.
25. S. Sengupta, N. S. Nichols, A. Del Maestro and V. N. Kotov, *Phys. Rev. Lett.*, 2018, **120**, 236802.
26. S. Nesic, R. Cuerno, E. Moro and L. Kondic, *Phys. Rev. E.*, 2015, **92**, 061002.
27. B. V. Derjaguin, N. V. Churaev and V. M. Muller, *Surface Forces*, Springer, New York, 1987.
28. B. V. Derjaguin and A. S. Titievskaya, *Prog. Surf. Sci.*, 1992, **40**, 64-73.
29. B. V. Derjaguin and A. S. Titijevskaya, *Prog. Surf. Sci.*, 1993, **43**, 74-82.
30. A. Sheludko, *Adv. Colloid Interface Sci.*, 1967, **1**, 391-464.
31. V. Bergeron, *J. Phys.: Condens. Matter*, 1999, **11**, R215-R238.
32. D. Fennell Evans and H. Wennerström, *The Colloidal Domain: Where Physics, Chemistry, Biology, and Technology Meet*, Wiley-VCH: New York, 2nd edn., 1999.
33. P. A. Kralchevsky, A. D. Nikolov, D. T. Wasan and I. B. Ivanov, *Langmuir*, 1990, **6**, 1180-1189.
34. R. von Klitzing, E. Thormann, T. Nylander, D. Langevin and C. Stubenrauch, *Adv. Colloid Interface Sci.*, 2010, **155**, 19-31.
35. D. T. Wasan and A. D. Nikolov, *Current Opinion in Colloid & Interface Science*, 2008, **13**, 128-133.
36. V. Bergeron and C. J. Radke, *Langmuir*, 1992, **8**, 3020-3026.
37. P. Oswald and P. Pieranski, *Smectic and Columnar Liquid Crystals: Concepts and Physical Properties Illustrated by Experiments*, CRC Press, 2005.
38. S. E. Anachkov, K. D. Danov, E. S. Basheva, P. A. Kralchevsky and K. P. Ananthapadmanabhan, *Adv. Colloid Interface Sci.*, 2012, **183**, 55-67.
39. A. Mamane, E. Chevallier, L. Olanier, F. Lequeux and C. Monteux, *Soft Matter*, 2017, **13**, 1299-1305.
40. P. J. Beltramo and J. Vermant, *ACS Omega*, 2016, **1**, 363-370.
41. P.-G. de Gennes and J. Badoz, *Fragile Objects: Soft Matter, Hard Science, and the Thrill of Discovery*, Springer-Verlag NewYork 1996.
42. G. Gochev, D. Platikanov and R. Miller, *Adv. Colloid Interface Sci.*, 2016, **233**, 115-125.
43. I. Cantat, S. Cohen-Addad, F. Elias, F. Graner, R. Höhler and O. Pitois, *Foams: Structure and Dynamics*, Oxford University Press, 2013.
44. C. V. Boys, *Soap Bubbles: Their Colours and the Forces Which Mold Them*, Society for Promoting Christian Knowledge, London, 1912.
45. K. J. Mysels, S. Frankel and K. Shinoda, *Soap films: Studies of their Thinning and a Bibliography*, Pergamon Press, 1959.
46. D. L. Weaire and S. Hutzler, *The Physics of Foams*, Oxford University Press, 1999.
47. R. I. Saye and J. A. Sethian, *Science*, 2013, **340**, 720-724.
48. C. Hill and J. Eastoe, *Adv. Colloid Interface Sci.*, 2017, **247**, 496-513.
49. V. Bergeron, A. I. Jimenez-Laguna and C. J. Radke, *Langmuir*, 1992, **8**, 3027-3032.
50. Y. Zhang and V. Sharma, *Soft Matter*, 2015, **11**, 4408-4417.
51. Y. Zhang, S. Yilixiati, C. Pearsall and V. Sharma, *ACS Nano*, 2016, **10**, 4678-4683.
52. Y. Zhang and V. Sharma, *Langmuir*, 2018, **34**, 1208-1217.
53. S. Yilixiati, R. Rafiq, Y. Zhang and V. Sharma, *ACS Nano*, 2018, **12**, 1050-1061.
54. Y. Zhang and V. Sharma, *Langmuir*, 2018, **34**, 7922–7931.

55. R. Hooke, *Micrographia: or Some Physiological Descriptions of Minute Bodies Made by Magnifying Glasses. With Observations and Inquiries Thereupon.*, London, 1665.
56. I. Newton, *Opticks: or, A Treatise of the Reflexions, Refractions, Inflexions and Colours of Light* London, 4th edn., 1706.
57. D. Brewster, *Proceedings of the Royal Society of Edinburgh*, 1869, **6**, 64-65.
58. J. N. Israelachvili, *Intermolecular and Surface Forces*, Academic Press, 3rd edn., 2011.
59. D. Langevin and A. A. Sonin, *Adv. Colloid Interface Sci.*, 1994, **51**, 1-27.
60. E. S. Johonnott, *Philosophical Magazine Series 6*, 1906, **11**, 746-753.
61. J. Perrin, *Ann. Phys. (Paris)*, 1918, **10**, 160-184.
62. J. Perrin, *Journal*, 1928.
63. H. G. Bruil and J. Lyklema, *Nature Physical Science*, 1971, **233**, 19.
64. S. Friberg, S. E. LINDEN and H. Saito, *Nature*, 1974, **251**, 494.
65. E. Manev, J. E. Proust and L. Ter-Minassian-Saraga, *Colloid. Polym. Sci.*, 1977, **255**, 1133-1135.
66. C. Y. Young, R. Pindak, N. A. Clark and R. B. Meyer, *Phys. Rev. Lett.*, 1978, **40**, 773.
67. E. B. Sirota, P. S. Pershan, L. B. Sorensen and J. Collett, *Phys. Rev. A*, 1987, **36**, 2890.
68. P. Pieranski, L. Beliard, J.-P. Tournellec, X. Leoncini, C. Furtlehner, H. Dumoulin, E. Riou, B. Jouvin, J.-P. Fénerol and P. Palaric, *Phys. A*, 1993, **194**, 364-389.
69. A. D. Nikolov, D. T. Wasan, P. A. Kralchevsky and I. B. Ivanov, Kyoto, Japan, 1988.
70. A. D. Nikolov and D. T. Wasan, *J. Colloid Interface Sci.*, 1989, **133**, 1-12.
71. A. D. Nikolov, P. A. Kralchevsky, I. B. Ivanov and D. T. Wasan, *J. Colloid Interface Sci.*, 1989, **133**, 13-22.
72. D. T. Wasan, A. D. Nikolov, P. A. Kralchevsky and I. B. Ivanov, *Colloids and Surfaces*, 1992, **67**, 139-145.
73. E. S. Basheva, K. D. Danov and P. A. Kralchevsky, *Langmuir*, 1997, **13**, 4342-4348.
74. P. A. Kralchevsky and N. D. Denkov, *Chem. Phys. Lett.*, 1995, **240**, 385-392.
75. G. N. Sethumadhavan, A. Nikolov and D. Wasan, *Langmuir*, 2001, **17**, 2059-2062.
76. A. D. Nikolov and D. T. Wasan, *Colloids and Surfaces a-Physicochemical and Engineering Aspects*, 1997, **123**, 375-381.
77. X. L. Chu, A. D. Nikolov and D. T. Wasan, *J. Chemical Physics*, 1995, **103**, 6653-6661.
78. A. A. Sonin and D. Langevin, *Europhys. Lett.*, 1993, **22**, 271.
79. C. M. Beltrán and D. Langevin, *Phys. Rev. Lett.*, 2005, **94**, 217803.
80. A. D. Nikolov, P. A. Kralchevsky, I. B. Ivanov and D. T. Wasan, *J. Colloid Interface Sci.*, 1989, **133**, 13-22.
81. J. Lee, A. Nikolov and D. Wasan, *Langmuir*, 2016, **32**, 4837-4847.
82. J. Lee, A. Nikolov and D. Wasan, *J. Colloid Interface Sci.*, 2017, **496**, 60-65.
83. J. Lee, A. D. Nikolov and D. T. Wasan, *J. Colloid Interface Sci.*, 2017, **487**, 217-222.
84. A. Oron, S. H. Davis and S. G. Bankoff, *Rev. Mod. Phys.*, 1997, **69**, 931.

85. L. n. Champougny, J. Miguet, R. Henaff, F. d. r. Restagno, F. o. Boulogne and E. Rio, *Langmuir*, 2018, **34**, 3221-3227.
86. A. Nikolov and D. Wasan, *J Colloid Interface Sci*, 1989, **133**, 1-12.
87. S. Yilixiati, R. Rafiq, Y. Zhang and V. Sharma, *ACS Nano*, 2018, **12**, 1050-1061.
88. Y. Zhang and V. Sharma, *Langmuir*, 2017.
89. V. Bergeron, D. Langevin and A. Asnacios, *Langmuir*, 1996, **12**, 1550-1556.
90. C. M. Beltran, S. Guillot and D. Langevin, *Macromolecules*, 2003, **36**, 8506-8512.
91. E. S. Basheva, P. A. Kralchevsky, K. D. Danov, K. P. Ananthapadmanabhan and A. Lips, *Phys. Chem. Chem. Phys.*, 2007, **9**, 5183-5198.
92. K. D. Danov, E. S. Basheva, P. A. Kralchevsky, K. P. Ananthapadmanabhan and A. Lips, *Adv. Colloid Interface Sci.*, 2011, **168**, 50-70.
93. L. Saulnier, L. Champougny, G. Bastien, F. Restagno, D. Langevin and E. Rio, *Soft matter*, 2014, **10**, 2899-2906.
94. L. Saulnier, F. Restagno, J. Delacotte, D. Langevin and E. Rio, *Langmuir*, 2011, **27**, 13406-13409.
95. S. Berg, E. A. Adelizzi and S. M. Troian, *Langmuir*, 2005, **21**, 3867-3876.
96. R. Bruinsma, *Physica A*, 1995, **216**, 59-76.
97. V. A. Nierstrasz and G. Frens, *J. Colloid Interface Sci.*, 1998, **207**, 209-217.
98. P. J. Flory, *Principles of Polymer Chemistry*, Cornell University Press, Ithaca, 1953.
99. F. S. Bates and P. Wiltzius, *J. Chem. Phys.*, 1989, **91**, 3258-3274.
100. M. Rubinstein and R. H. Colby, *Polymer Physics*, Oxford Univ. Press: New York, 2003.
101. R. G. Larson, *The Structure and Rheology of Complex Fluids*, Oxford University Press, New York, 1999.
102. T. Hashimoto, M. Itakura and H. Hasegawa, *J. Chem. Phys.*, 1986, **85**, 6118-6128.
103. N. F. Carnahan and K. E. Starling, *J. Chem. Phys.*, 1969, **51**, 635-636.
104. Y. Couder, J. M. Chomaz and M. Rabaud, *Physica D*, 1989, **37**, 384-405.
105. J. B. M. Hudales and H. N. Stein, *J. Colloid Interface Sci.*, 1990, **138**, 354-364.
106. A. Aradian, E. Raphael and P. G. de Gennes, *Europhys. Lett.*, 2001, **55**, 834-840.